18. J. M. Mason *et al.*, *Cancer Cell* **26**, 163–176 (2014).
19. P. B. Sampson *et al.*, *J. Med. Chem.* **58**, 147–169 (2015).
20. D. A. Sloane *et al.*, *ACS Chem. Biol.* **5**, 563–576 (2010).
21. R. M. Rios, *Philos. Trans. R. Soc. Lond. B Biol. Sci.* **369**, 20130462 (2014).
22. A. Khodjakov, C. L. Rieder, *J. Cell Biol.* **153**, 237–242 (2001).
23. J. H. Sir *et al.*, *J. Cell Biol.* **203**, 747–756 (2013).
24. Y. Uetake *et al.*, *J. Cell Biol.* **176**, 173–182 (2007).
25. L. M. Jenkins, S. R. Durell, S. J. Mazur, E. Appella, *Carcinogenesis* **33**, 1441–1449 (2012).
26. N. D. Lakin, S. P. Jackson, *Oncogene* **18**, 7644–7655 (1999).
27. N. J. Ganem *et al.*, *Cell* **158**, 833–848 (2014).
28. Y. Uetake, G. Sluder, *Curr. Biol.* **20**, 1666–1671 (2010).
29. H. Bazzi, K. V. Anderson, *Proc. Natl. Acad. Sci. U.S.A.* **111**, E1491–E1500 (2014).
30. D. Izquierdo, W. J. Wang, K. Uryu, M. F. Tsou, *Cell Reports* **8**, 957–965 (2014).
31. H. Shen, C. G. Maki, *Curr. Pharm. Des.* **17**, 560–568 (2011).
32. R. Basto *et al.*, *Cell* **125**, 1375–1386 (2006).
33. F. Bartolini, G. G. Gundersen, *J. Cell Sci.* **119**, 4155–4163 (2006).
34. M. Stiess *et al.*, *Science* **327**, 704–707 (2010).
35. K. D. Sumigray, T. Lechler, *BioArchitecture* **1**, 221–224 (2011).

ACKNOWLEDGMENTS

We thank Z. Li for leading the Sundia Meditech chemistry team, Advanced Photon Source NE-CAT (supported by NIH GM103403) for assistance with x-ray data collection, Q. Zhu and I. Verma for the p53 and Glu4 shRNA lentiviruses, A. Holland and D. Cleveland for the Plk4-YFP DLD-1 cell line, R. Gassmann for help with initial cell-based assays, M. Kaulich for technical advice on CRISPR/Cas9, and A. Dammermann for generation of the Sas6 and Cep192 antibodies. J.V.A, R.L.D., M.Y., A.M., C.P.S., J.E.H., A.D., T.C.G., A.K.S., and K.O. receive salary and other support from the Ludwig Institute for Cancer Research. This work was supported by NIH grants to K.O. (GM074207) and B.J.M. (GM089970), and with funds from the Hilton Ludwig Cancer Prevention Initiative to A.K.S. and T.C.G. The data described here are tabulated in the main paper and Supplementary Materials. The structure of the centrinone-bound Plk4 kinase domain complex has been deposited in the Protein Data Bank (4YUR). The Ludwig Institute for Cancer Research has filed a patent application (62/149,292) related to the structures, syntheses, and uses of centrinone, centrinone B, and chemically related Plk4 inhibitors. Requests for the centrinones should be directed to A.K.S. (ashiau@ucsd.edu).

SUPPLEMENTARY MATERIALS

www.sciencemag.org/content/348/6239/1155/suppl/DC1
Materials and Methods
Figs. S1 to S14
Tables S1 to S6
References (*36*–*63*)

17 December 2014; accepted 17 April 2015
Published online 30 April 2015;
10.1126/science.aaa5111

AGING STEM CELLS

A Werner syndrome stem cell model unveils heterochromatin alterations as a driver of human aging

Weiqi Zhang,[1]* Jingyi Li,[2]* Keiichiro Suzuki,[3]* Jing Qu,[4]* Ping Wang,[1] Junzhi Zhou,[1] Xiaomeng Liu,[2] Ruotong Ren,[1] Xiuling Xu,[1] Alejandro Ocampo,[3] Tingting Yuan,[1] Jiping Yang,[1] Ying Li,[1] Liang Shi,[5] Dee Guan,[1] Huize Pan,[1] Shunlei Duan,[1] Zhichao Ding,[1] Mo Li,[3] Fei Yi,[6] Ruijun Bai,[4] Yayu Wang,[5] Chang Chen,[1] Fuquan Yang,[1] Xiaoyu Li,[7] Zimei Wang,[8] Emi Aizawa,[3] April Goebl,[3,9] Rupa Devi Soligalla,[3] Pradeep Reddy,[3] Concepcion Rodriguez Esteban,[3] Fuchou Tang,[2,10,11,12]† Guang-Hui Liu,[1,8,11,13]† Juan Carlos Izpisua Belmonte[3]†

Werner syndrome (WS) is a premature aging disorder caused by WRN protein deficiency. Here, we report on the generation of a human WS model in human embryonic stem cells (ESCs). Differentiation of WRN-null ESCs to mesenchymal stem cells (MSCs) recapitulates features of premature cellular aging, a global loss of H3K9me3, and changes in heterochromatin architecture. We show that WRN associates with heterochromatin proteins SUV39H1 and HP1α and nuclear lamina–heterochromatin anchoring protein LAP2β. Targeted knock-in of catalytically inactive *SUV39H1* in wild-type MSCs recapitulates accelerated cellular senescence, resembling WRN-deficient MSCs. Moreover, decrease in WRN and heterochromatin marks are detected in MSCs from older individuals. Our observations uncover a role for WRN in maintaining heterochromatin stability and highlight heterochromatin disorganization as a potential determinant of human aging.

Werner syndrome (WS), also known as adult progeria, recapitulates certain aspects of human physiological aging (*1*). WS is caused by mutations in the *WRN* gene, resulting in loss of WRN expression or function (*1*). WRN protein plays roles in DNA replication, transcription, repair, and recombination, as well as telomere maintenance, indicating that one of the major causes for WS pathogenesis relates to genomic instability (*1*, *2*). Epigenetic alterations have been associated with cellular aging in diverse model organisms (*2*–*4*). In humans, somatic cells derived from patients with premature aging syndromes are characterized by loss of heterochromatin marks (*5*–*7*). However, it is unclear whether epigenetic dysregulation is involved in WS pathogenesis.

Generation of patient-specific induced pluripotent stem cells (iPSCs) represents a promising avenue to model and study human aging and aging-associated disorders (*8*). WS-specific iPSC lines may constitute an ideal source for in vitro modeling of WS. However, we found that WS patient fibroblast lines deposited in different cell banks presented severe karyotypic abnormalities and secondary DNA mutations associated with advanced stages of WS pathology. To create an unbiased human WS cellular model, we sought to generate an isogenic WS embryonic stem cell (ESC) line by knocking out exons 15 and 16 of the *WRN* gene encoding the conserved DNA helicase domain (*9*). After two rounds of homologous recombination using helper-dependent adenoviral vector (HDAdV) (*10*, *11*), we successfully generated homozygous *WRN*-null ESC lines (ESCs-*WRN*$^{-/-}$) (Fig. 1, A and B, and fig. S1, A to D). ESCs-*WRN*$^{-/-}$ expressed pluripotency markers, maintained normal karyotype, and could differentiate into all three germ layers (Fig. 1A and fig. S2, A to E). ESCs-*WRN*$^{-/-}$ lacked detectable WRN protein, as determined by Western blot using antibodies specific to the N or C terminus of WRN (Fig. 1B). No difference in cell cycle kinetics and cell growth rate between wild-type and WRN-null ESCs was observed (fig. S2, F to H).

WS patients are mainly characterized by premature aging pathologies associated with degeneration of mesodermal tissues, i.e., osteoporosis, atherosclerosis, and gray hair (*1*). We hypothesized that WS patients may suffer from an accelerated exhaustion of the mesenchymal stem cell (MSC) pool. This was tested by differentiating ESCs-*WRN*$^{-/-}$ into MSCs. MSCs-*WRN*$^{-/-}$ expressed MSC-specific cell surface markers CD73, CD90, CD105; lacked expression of MSC-irrelevant antigens, including CD45, CD34, and CD43 (fig. S3A); and

[1]National Laboratory of Biomacromolecules, Institute of Biophysics, Chinese Academy of Sciences, Beijing 100101, China. [2]Biodynamic Optical Imaging Center, College of Life Sciences, Peking University, Beijing 100871, China. [3]Gene Expression Laboratory, Salk Institute for Biological Studies, 10010 North Torrey Pines Road, La Jolla, CA 92037, USA. [4]State Key Laboratory of Reproductive Biology, Institute of Zoology, Chinese Academy of Sciences, Beijing 100101, China. [5]Diagnosis and Treatment Center for Oral Disease, the 306th Hospital of the PLA, Beijing, China. [6]Department of Molecular and Cellular Physiology, Stanford University School of Medicine, Stanford, CA 94305, USA. [7]College of Life Sciences, Peking University, Beijing 100871, China. [8]The Center for Anti-aging and Regenerative Medicine, Shenzhen University, Shenzhen 518060, China. [9]Universidad Católica San Antonio de Murcia, Campus de los Jerónimos s/n, 30107 Guadalupe, Murcia, Spain. [10]Ministry of Education Key Laboratory of Cell Proliferation and Differentiation, Beijing 100871, China. [11]Center for Molecular and Translational Medicine (CMTM), Beijing 100101, China. [12]Peking-Tsinghua Center for Life Sciences, Peking University, Beijing 100871, China. [13]Beijing Institute for Brain Disorders, Beijing 100069, China.
*These authors contributed equally to this work. **†Corresponding author. E-mail: ghliu@ibp.ac.cn (G.-H.L.); tangfuchou@pku.edu.cn (F.T.); belmonte@salk.edu (J.C.I.B.)**

could differentiate into osteoblasts, chondrocytes, and adipocytes (fig. S3, B and C) (*12*).

Upon serial passaging, WRN-deficient MSCs recapitulated major phenotypes of premature aging, including premature loss of proliferative potential, increased number of senescence-associated–β-galactosidase (SA-β-gal)–positive cells, up-regulated expression of aging-associated genes $p16^{Ink4a}$ and $p21^{Waf1}$, and activation of senescence-associated secretory phenotype (SASP) (Fig. 1, C to E, and fig. S3, D to G) (*13*). Moreover, when WRN-deficient MSCs expressing luciferase were transplanted into the muscle of nonobese diabetic/severe combined immunodeficiency (NOD/SCID) mice, they underwent an accelerated attrition compared to wild-type MSCs (Fig. 1F and fig. S3H). These results demonstrated that the loss of WRN promotes premature senescence in MSCs.

WRN deficiency in MSCs resulted in elevated DNA damage response (DDR), indicated by increased nuclear foci for 53BP1, γ-H2AX, and phosphorylated ATM/ATR substrates (fig. S4, A to C). Restoration of WRN activity by lentivirus-mediated expression in MSCs-$WRN^{-/-}$ resulted in partial alleviation of DDR and cellular senescence (fig. S4, D and E). To investigate potential chromosomal abnormalities resulting from the loss of WRN protein, we performed genome-wide copy number variation (CNV) analysis by deep sequencing. In the time frame examined, genomic integrity was minimally affected in MSCs-$WRN^{-/-}$ (fig. S4F).

Epigenetic alteration has been considered as a hallmark of aging (*2*). MSCs-$WRN^{-/-}$ showed a distinct nuclear Hoechst 33342 staining pattern with markedly enlarged nuclei and a high pixel-to-pixel coefficient of variation (CV) value, indicating possible changes in chromatin structure (Fig. 2A and fig. S5A). Moreover, WRN-deficient MSCs exhibited accelerated diminishment of heterochromatin-associated inner nuclear membrane (INM) proteins LAP2β and LBR and reduced heterochromatin structure underneath the nuclear envelope, as indicated by immunostaining and electron microscopy (Fig. 2B and fig. S5, B and C) (*14*). These results suggest a progressive disorganization of heterochromatin in WRN-deficient MSCs.

Further investigation of heterochromatin reorganization at histone and DNA levels revealed marked down-regulation of the constitutive heterochromatin mark H3K9me3 (trimethylated histone H3 at lysine-9) in MSC-$WRN^{-/-}$ (Fig. 2C and fig. S5, D and E). In contrast, H3K27me3 showed slight down-regulation, whereas H3K4me3, a mark for euchromatin fiber, exhibited comparable levels between WRN-deficient and wild-type MSCs (Fig. 2C and fig. S5, D and E). We did not observe obvious genome-wide alteration of 5-methylcytosine (5mC) in WRN-deficient MSCs (Fig. 2C). Bioinformatic analysis identified 73 H3K9me3-enriched "mountains" throughout the genome in MSCs-$WRN^{+/+}$, which are characterized by >20 kb of consecutive peaks of H3K9me3 (Fig. 2D). Of these H3K9me3 mountains, 28 (38%) were lost in MSCs-$WRN^{-/-}$ (Fig. 2D). Interestingly, 24 (86%) of these impaired H3K9me3 mountains resided in subtelomeric or subcentromeric regions (Fig. 2, D and E, and table S1).

RNA sequencing (RNA-seq) identified 1047 RefSeq genes that showed differential expression in MSCs-$WRN^{-/-}$ (fig. S6, A and B, and table S2). The most obviously down-regulated genes were centromere-packaging proteins and components of the nuclear membrane (fig. S6, A to E, and table S3). These results indicate alterations in nuclear structure and epigenomic organization, potentially leading to a progressive loss of heterochromatin structure in MSCs as a consequence of WRN depletion.

In agreement with previous reports describing WRN as a telomere-associated protein required for telomere maintenance (*15*), compromised telomerase activity and shorter telomere length were detected in MSC-$WRN^{-/-}$ (fig. S7, A and B). In addition, chromatin immunoprecipitation–quantitative polymerase chain reaction (ChIP-QPCR) showed binding of WRN to the H3K9me3-enriched centromeric loci α-Satellite (α-Sat) and Satellite 2 (Sat2) (Fig. 3A) (*16*). Depletion of WRN resulted in an increase in centromeric γ-H2AX signal and a loss of H3K9me3 from α-Sat and Sat2 loci accompanied by up-regulation of transcripts from these sequences (Fig. 3, A and B, and fig. S7C). Coimmunoprecipitation (Co-IP) analysis revealed WRN as part of a complex containing the major histone methyltransferase for H3K9me3—SUV39H1, HP1α, and LAP2β, a nuclear envelope component that recruits heterochromatin via anchoring to HP1α (Fig. 3C and fig. S7D) (*17*). These observations suggest a role for WRN, together with SUV39H1 and HP1α, in the stabilization of heterochromatin.

We next tested whether disorganization of heterochromatin could contribute to accelerated cellular senescence. Knockdown of SUV39H1 or HP1α in wild-type MSCs led to a reduction of overall H3K9me3 and induction of cellular senescence, as assayed by Western blot, SA-β-gal staining, and p16 expression (Fig. 3D and fig. S8, A to D). On the contrary, overexpression of HP1α up-regulated H3K9me3 levels and repressed cellular senescence in WRN-deficient MSCs (fig. S8, E to H). To confirm these observations, we

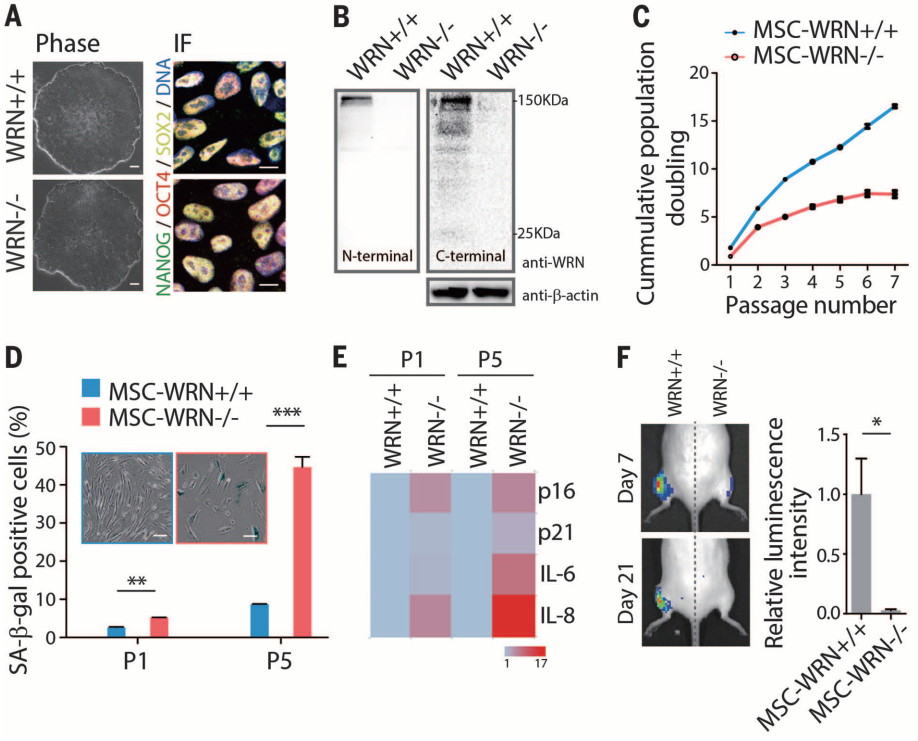

Fig. 1. WRN-deficient MSCs exhibit phenotypes associated with premature cellular senescence. (**A**) Morphology and immunofluorescence (IF) analyses of pluripotency markers in ESCs. Scale bar, 100 μm and 10 μm, respectively. (**B**) Western blot analysis of WRN expression in ESCs using anti-WRN N-terminal (ab200) and C-terminal (SC-5629) antibodies. (**C**) Growth curve analyzing the cumulative population doubling of MSCs. (**D**) Senescence-associated (SA)–β-gal staining in passage 1 (P1) and P5 MSCs. Scale bar, 50 μm. (**E**) Quantitative RT-PCR analysis of the indicated genes in P1 and P5 MSCs. Transcript levels were normalized to MSCs-$WRN^{+/+}$ group. Genes with greater mean value are color coded toward red. (**F**) Photon flux from muscle of a NOD-SCID mouse transplanted with MSCs-$WRN^{+/+}$ (left) and MSCs-$WRN^{-/-}$ (right) expressing luciferase. All data are represented as mean + SEM. $^{*}P < 0.05$, $^{**}P < 0.01$, $^{***}P < 0.001$ by Student's *t* test; $n = 3$ independent experiments.

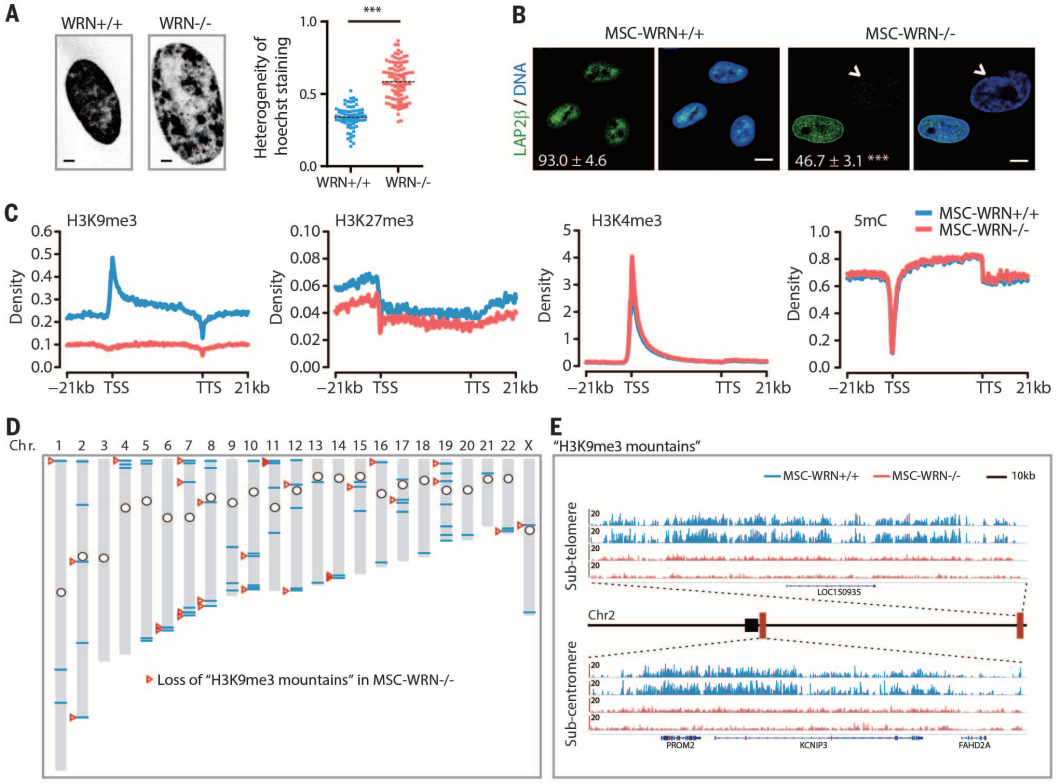

Fig. 2. Epigenomic analyses of WRN-deficient MSCs. (**A**) Left: Chromatin structure of MSCs shown by Hoechst 33342 staining of the nucleus. Scale bar, 5 μm. Right: CV value of nuclear Hoechst staining intensity used to evaluate the heterogeneity (pixel-to-pixel variation) of Hoechst intensity. (**B**) Immunofluorescence analyses of LAP2β expression in MSC-*WRN*$^{+/+}$ and MSC-*WRN*$^{-/-}$ at P5. Arrowheads denote abnormal nuclei with decreased LAP2β expression (percentage of LAP2β–positive nuclei in corner). Scale bar, 10 μm. n = 3 independent experiments. (**C**) Enrichment of H3K9me3, H3K27me3, H3K4me3, and 5mC on the gene bodies and 21 kb upstream of TSS (transcription start site) and 21 kb downstream of TTS (transcription terminal site) regions in the human genome. (**D**) Sketch map of "H3K9me3 mountain" distribution over 23 chromosomes. The blue lines indicate 73 "H3K9me3 mountains" present in MSCs-*WRN*$^{+/+}$, whereas 48 (65.8%) of them are localized within 5 Mb regions around the telomeres or centromeres. The red arrowheads indicate 28 "H3K9me3 mountains," which are lost in MSCs-*WRN*$^{-/-}$. The circles indicate the centromeres of chromosomes. (**E**) Representative images showing two "H3K9me3 mountains" on chromosome 2 in the subtelomere or subcentromere regions in P5 MSCs-*WRN*$^{-/-}$ and MSCs-*WRN*$^{+/+}$. Two biological replicates of each sample are presented. Black square denotes the centromere; red rectangles denote the position of the presented subtelomere and subcentromere regions, respectively. All data are represented as mean + SEM. ***P < 0.001 by Student's t test.

Fig. 3. WRN associates with centromeric heterochromatin and forms a molecular complex with SUV39H1 and HP1α. (**A**) Enrichment of WRN and H3K9me3 within the region of α-Sat or Sat2 as measured by ChIP-qPCR. (**B**) Quantitative RT-PCR analysis of centromeric repetitive element transcripts in MSCs at the indicated passages. (**C**) Left, coimmunoprecipitation of SUV39H1, HP1α, and LAP2β protein with endogenous WRN protein; Right, co-immunoprecipitation of WRN and HP1α with endogenous SUV39H1 in wild-type MSCs. (**D**) SA-β-gal staining (left) and p16 transcript (right) analyses in wild-type MSCs transduced with control lentiviral vector (CTRL) or lentiviral vector encoding for the indicated short hairpin RNA (Knock-down). All data are represented as mean + SEM. *P < 0.05, **P < 0.01, and ***P < 0.001 by Student's t test; n = 3 independent experiments.

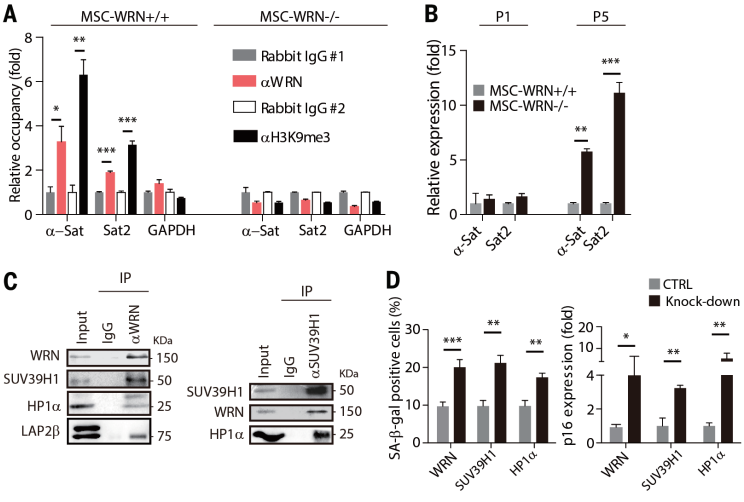

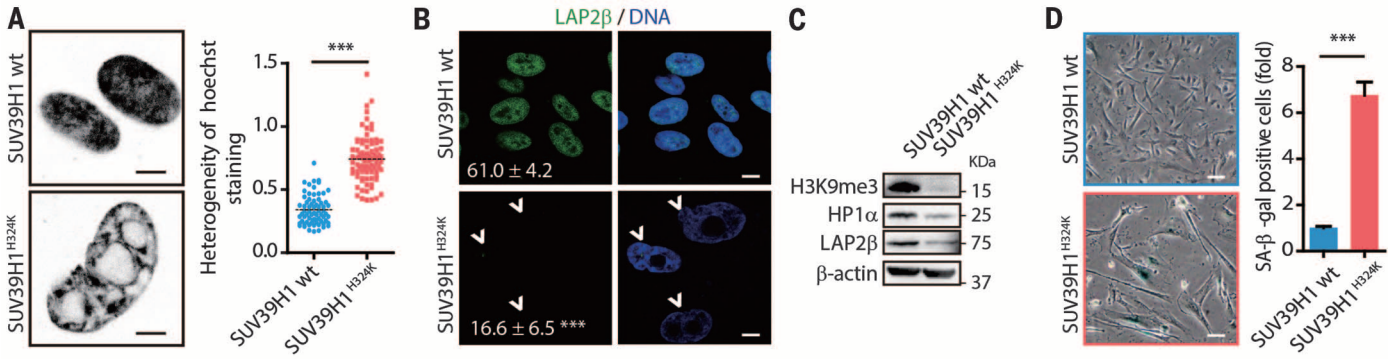

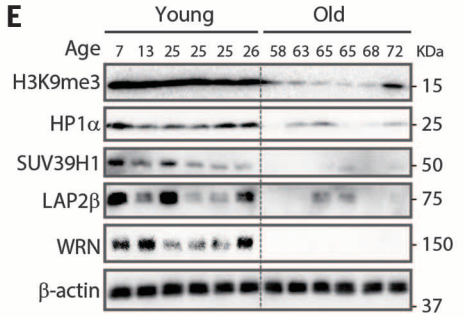

Fig. 4. *SUV39H1*^{H324K} mutant MSCs exhibit defective nuclear envelope and heterochromatin, as well as phenotypes of premature cellular senescence. (**A**) As described in Fig. 2A (left), Hoechst staining images of the nucleus; right, CV value of nuclear Hoechst staining intensity used to evaluate the heterogeneity (pixel-to-pixel variation) of Hoechst intensity. (**B**) Immunofluorescence analyses of LAP2β expression in MSCs. Arrowheads denote the abnormal nuclei with decreased LAP2β (percentages of normal nuclei presented at corner). Scale bar, 20 μm. $n = 3$ independent experiments. (**C**) Western blot analysis of the indicated proteins in MSCs. (**D**) SA-β-gal staining in MSCs at P5. Scale bar, 50 μm. $n = 3$ independent experiments. (**E**) Western blot analysis of the indicated proteins in human primary MSCs derived from old and young healthy individuals at P4 (see table S4). All data are represented as mean + SEM. ***$P < 0.001$ by Student's t test.

generated pluripotent ESCs-*SUV39H1*^{H324K} lines harboring catalytically inactivated endogenous SUV39H1 (fig. S9, A to D). Upon differentiation, MSCs-*SUV39H1*^{H324K} displayed drastic nuclear structural and chromosomal changes, loss of INM proteins LAP2β and LBR, decreased levels of H3K9me3 and HP1α, up-regulation of centromeric repetitive sequence transcription, and coordinated transcriptional down-regulation of centromere-packaging components (Fig. 4, A to C, and fig. S10, A and B). MSCs-*SUV39H1*^{H324K} recapitulated premature aging phenotypes observed in WRN-deficient MSCs, including retarded cell growth and accelerated cellular senescence determined by SA-β-gal staining (Fig. 4D and fig. S10, C to E). High expression of SUV39H2, a germline-specific histone methyltransferase, and/or other factors may functionally compensate for SUV39H1 deficiency in ESCs (fig. S10F) (*18*, *19*), where upon inactivation of the WRN-SUV39H1 axis, no discernible heterochromatin change was observed (figs. S10G and S8A). It should be noted that MSCs-*SUV39H1*^{H324K} exhibit neither increased γ-H2AX ($P = 0.773$) and phosphorylated ATM/ATR substrates ($P = 0.279$), nor telomere attrition (figs. S10H and S7, A and B). These results indicate that heterochromatin destabilization promotes premature aging in MSCs.

Finally, we asked whether heterochromatin disorganization could be a common hallmark for physiological human stem cell aging. For this purpose, we compared the levels of heterochromatin marks in primary dental pulp MSCs derived from six young (7- to 26-year-old) and six old (58- to 72-year-old) individuals (fig. S10I and table S4) (*20*). A marked down-regulation of WRN protein associated with a decrease in H3K9me3, HP1α, SUV39H1, and LAP2β levels in MSCs derived from old individuals (Fig. 4E). Therefore, specific heterochromatin changes may underlie both pathological and physiological MSC aging.

In summary, we have found that WRN protein, besides its role in DNA repair, functions to safeguard heterochromatin stability (fig. S11). Our results reveal that the progressive heterochromatin disorganization observed in WRN-deficient MSCs underlies cellular aging, but more extensive studies are needed to examine its role during physiological aging. The methodologies and observations introduced here may be used and extended toward the systematic study of other age-associated molecular events with relevance to human aging and age-related disorders.

REFERENCES AND NOTES

1. B. A. Kudlow, B. K. Kennedy, R. J. Monnat Jr., *Nat. Rev. Mol. Cell Biol.* **8**, 394–404 (2007).
2. C. López-Otín, M. A. Blasco, L. Partridge, M. Serrano, G. Kroemer, *Cell* **153**, 1194–1217 (2013).
3. G. Pegoraro *et al.*, *Nat. Cell Biol.* **11**, 1261–1267 (2009).
4. E. L. Greer *et al.*, *Nature* **466**, 383–387 (2010).
5. G.-H. Liu *et al.*, *Nature* **472**, 221–225 (2011).
6. D. K. Shumaker *et al.*, *Proc. Natl. Acad. Sci. U.S.A.* **103**, 8703–8708 (2006).
7. J. D. Miller *et al.*, *Cell Stem Cell* **13**, 691–705 (2013).
8. G. H. Liu, Z. Ding, J. C. Izpisua Belmonte, *Curr. Opin. Cell Biol.* **24**, 765–774 (2012).
9. D. B. Lombard *et al.*, *Mol. Cell. Biol.* **20**, 3286–3291 (2000).
10. G.-H. Liu *et al.*, *Nature* **491**, 603–607 (2012).
11. K. Suzuki *et al.*, *Cell Stem Cell* **15**, 31–36 (2014).
12. G. H. Liu *et al.*, *Nat. Commun.* **5**, 4330 (2014).
13. F. Rodier, J. Campisi, *J. Cell Biol.* **192**, 547–556 (2011).
14. T. Dechat, S. A. Adam, P. Taimen, T. Shimi, R. D. Goldman, *Cold Spring Harb. Perspect. Biol.* **2**, a000547 (2010).
15. A. S. Multani, S. Chang, *J. Cell Sci.* **120**, 713–721 (2007).
16. D. Wang *et al.*, *Proc. Natl. Acad. Sci. U.S.A.* **110**, 5516–5521 (2013).
17. N. Kourmouli *et al.*, *EMBO J.* **19**, 6558–6568 (2000).
18. D. O'Carroll *et al.*, *Mol. Cell. Biol.* **20**, 9423–9433 (2000).
19. W. Zhang, J. Qu, K. Suzuki, G.-H. Liu, J. C. Izpisua Belmonte, *Trends Cell Biol.* **23**, 587–592 (2013).
20. G. B. Tomar *et al.*, *Biochem. Biophys. Res. Commun.* **393**, 377–383 (2010).

ACKNOWLEDGMENTS

We are grateful to W. G. Zhu, L. Comai, K. Mitani, P. Ng, and A. Lieber for sharing experimental materials; L. Sun, W. Ding, G. Yuan, and X. Zhu from Center for Biological Imaging for technical assistance; and M. Schwarz and L. Zhao for administrative help. This work was supported by National Natural Science Foundation of China (NSFC: 81330008), National Basic Research Program of China (973 Program, 2015CB964800; 2014CB910500; 2014CB964600; 2012CB966704), the Strategic Priority Research Program of the Chinese Academy of Sciences (XDA01020312), NSFC (31222039; 31201111; 81371342; 81300261; 81300677; 81271266; 81471414; 81422017; 81401159; 31322037; 81471407), National High Technology Research and Development Program of China (863 program: 2015AA020307), Beijing Natural Science Foundation (7141005; 5142016), Key Research Program of the Chinese Academy of Sciences (KJZDEW-TZ-L05), the Thousand Young Talents program of China, National Laboratory of Biomacromolecules (012kf02;2013kf05;2013kf11;2014kf02;2015kf10) and State Key Laboratory of Drug Research (SIMM1302KF-17), and China Postdoctoral Science Foundation Grant (2013M530751). K.S and M.L. are supported by a California Institute for Regenerative Medicine Training Grant. A.O. was partially supported by an NIH Ruth L. Kirschstein National Research Service Award Individual Postdoctoral Fellowship. The physiological human cell aging studies were supported by UCAM. The J.C.I.B. laboratory was supported by The Glenn Foundation, The G. Harold and Leila Y. Mathers Charitable Foundation, and The Leona M. and Harry B. Helmsley Charitable Trust (2012-PG-MED002). All materials are available from the G.-H.L., F.T., and J.C.I.B. laboratories under a material transfer agreement with Institute of Biophysics (CAS), Peking University, or The Salk Institute for Biological Studies. Myc-HP1α plasmid can be obtained from W. G. Zhu under a material transfer agreement with Peking University.

SUPPLEMENTARY MATERIALS

www.sciencemag.org/content/348/6239/1160/suppl/DC1
Material and Methods
Figs. S1 to S11
Table S1 to S5
References (*21*–*47*)

21 October 2014; accepted 15 April 2015
Published online 30 April 2015;
10.1126/science.aaa1356

Science
AAAS

A Werner syndrome stem cell model unveils heterochromatin alterations as a driver of human aging

Weiqi Zhang *et al.*

Science **348**, 1160 (2015);
DOI: 10.1126/science.aaa1356

Science (print ISSN 0036-8075; online ISSN 1095-9203) is published weekly, except the last week in December, by the American Association for the Advancement of Science, 1200 New York Avenue NW, Washington, DC 20005.